Title: Mechanobiology of the Cell Membrane

Authors: Peter J Butler, PhD *

Hari Muddana, PhD **

Sara Farag, M.D. ***

Affiliations: * Department of Biomedical Engineering, The Pennsylvania State University, ** Department of Pharmacology, University of California San Diego, *** Obstetrics & Gynecology, Hershey Medical College, The Pennsylvania State University

Date: November 27, 2013

Introduction

In this chapter, we introduce the main concepts in membrane mechanics through an exploration of the relationship between mechanics and protein activation. Proteins can be activated by bringing them together, or by changing their conformation. So the question arises, can forces on membranes cause changes in transport of membrane components, such as proteins and lipids, and can forces cause changes in integral membrane protein conformation that are equivalent to those caused by ligand binding, a process well known to initiate biochemical signaling? The answers to these questions have significant implications in the field of mechanobiology because many of the important proteins that transduce external cellular signals to intracellular changes in signaling pathways and genetic expression reside in the plasma membrane.

The chapter begins with an overview of membrane composition and how this composition leads to unique mechanical properties of membranes. These mechanical properties are then described in terms of moduli and the principle equations describing the relationship between stress, strain, curvature, and membrane material properties are presented. We then present a link between membrane stress and protein activation using a series of theoretical models that quantify the free energy arising from hydrophobic mismatch between proteins and test whether this free energy is sufficient for protein activation. Next, we show how continuum membrane mechanics emerges from interactions of molecules using an example wherein membrane tension is applied to a molecular dynamics simulation of a lipid bilayer. Such changes in diffusion and lipid packing are measured experimentally using single molecule

fluorescence. With this background in mind, we present experimental evidence that membrane stress can lead to protein activation and changes in transport. Such studies represent a confluence of membrane mechanics, membrane composition, lateral transport, and mechanotransduction in focal adhesions.

Membrane organization arises from the amphiphilic nature of lipids

Lipids are amphiphilic molecules that self-assemble into ~ 5 nm thick cellular membranes. Such membranes function as semipermeable barriers between cell cytosol and extracellular material and compartmentalize internal organelles. Biological membranes harbor many proteins (nearly 30% of the genes expressed in animal cells (124)) that play essential roles in cellular function. Such functions include maintaining ion gradients across the membrane (e.g. ion channels), transduction of information from outside the cell to the cytosol through receptor activation (e.g. G-protein signaling), formation of structural connections between cell cytoskeleton and extracellular matrix (e.g. integrins), and communication between cells through junctional proteins (e.g. cadherins and connexins). In the famous fluid-mosaic model (111) Singer and Nicholson defined the lipid bilayer as a two-dimensional viscous solution with integral proteins. Since that original insight, our understanding of the lipid bilayer structure and its active role in regulating protein activity has developed significantly (28, 55, 110). Lipids are no longer considered as passive structural elements of cell membranes. Rather, they govern membrane protein activity through direct action on proteins, through their influence on structural properties of the bilayer, and through lipid metabolism. Importantly, understanding the interrelationship between structure and function of lipid bilayers and downstream signal

transduction underlies the development of novel biotherapeutic agents (80) against diseases that find their origins in lipid-protein interaction.

Membrane lipids in eukaryotic cells can be broadly classified into glycerolphospholipids and sphingolipids. The majority of the lipids in the eukaryotic cell membranes belong to the class of glycerophospholipids, that include phosphatidylcholines (PC), phosphatidylserine (PS), phosphatidylethanolamine (PE), and phosphotidylinositol (PI), of which PC is the major class comprising more than 50% of the total lipid content in cells (88). These lipid types have a common glycerol backbone and differ in the chemical nature of the head group. As a general feature, all lipids are amphiphilic with a polar (hydrophilic) head group region and a non-polar (hydrophobic) hydrocarbon tail region (schematic shown in Figure 1). Due to the amphiphilic nature, most lipids spontaneously aggregate to form double layers (i.e. bilayers) under aqueous conditions resulting in a two-dimensional planar structure. Depending on the geometry of the molecule (e.g. diacyl versus monoacyl lipids), they might also form micellar structures (Figure 1).

Another key molecular component of biological membranes is cholesterol. Cholesterol is unique to eukaryotic cell membranes and is the principal sterol synthesized in animal cells. Cholesterol is also an amphiphilic molecule that is largely hydrophobic with a rigid ring structure and a polar hydroxyl head group (Figure 1). Cholesterol plays several structural and functional roles in biological membranes (64). Cholesterol regulates membrane protein activity through specific sterol-protein interactions, by altering the bilayer's physical properties, and through self-organization of the bilayer into domains (18).

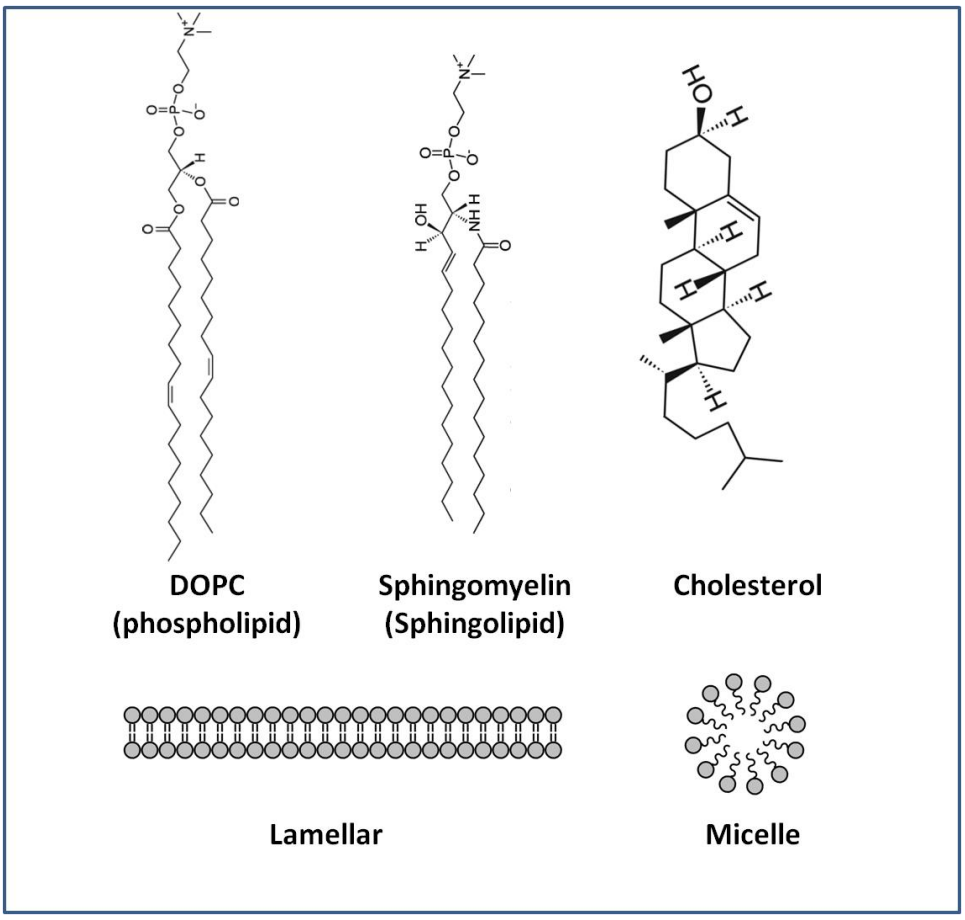

Figure 1: Chemical structures of phospholipids, sphingolipids, and cholesterol. Lipids adopt lamellar or micellar phases depending on whether their shape is optimal for planar or highly curved membranes as shown in the bottom panel.

Specific cholesterol binding sites have been identified for several membrane proteins including G-protein coupled receptors (46, 93, 94), ligand-gated ion channels (57), for inwardly rectifying potassium channels (112, 113) and large conductance calcium and potassium channels (27). Specific sterol-protein interactions are thought to modulate the functioning of these membrane proteins (18, 64). Cholesterol can also indirectly modulate protein activity by maintaining

certain physical properties of the lipid bilayer. For example, membrane cholesterol content has been shown to modulate volume-regulated anion current in endothelial cells, and this effect was reversed by replacing cholesterol with its chiral analogues, (68, 103) indicating modulation of protein activity through bilayer fluidity changes. Finally, cholesterol is an essential ingredient for lateral organization of lipid membranes into membrane domains (or rafts) (62).

Even though, macroscopically, the lipid bilayer is thought of as a two-dimensional continuous fluid, microscopically, it exhibits high asymmetry from one leaflet to the other and significant heterogeneity in the lateral direction. The inner and outer leaflets have asymmetric distribution in lipid composition with the outer leaflet enriched in phosphotidylcholines and sphingomyelins and the inner leaflet enriched in phosphotidylserines and phosphotidylethanolamines (26) with much of this asymmetry maintained by flipases, proteins that enable the "flipping" of polar head groups across the inner membrane hydrophobic barrier to the opposite leaflet. Cell membranes also exhibit highly complex self-organization in the lateral dimension, with regions enriched in sphingomyelin and cholesterol and regions enriched with poly-unsaturated phosphotidylcholines and depleted of cholesterol (78). Such compositional heterogeneity implies that mechanical properties are heterogeneous as well, with areas of high and low compressibility moduli (119) .

The wide variety of lipids gives rise to bilayers of various crystalline phases including gel, ripple, and liquid (liquid disordered (L_d), and liquid ordered (L_o)) (72). In the gel phase, the hydrocarbon chains are arranged in an all-trans state, whereas in the liquid state they undergo fast *trans* to *gauche* transformations resulting in high fluidity. The transition of the gel phase to

liquid phase happens at a specific temperature, referred as phase transition temperature. The phase transition temperature of a lipid is governed by its chemical structure and is predominantly affected by the length and degree of saturation of the hydrocarbon chains. For example, the phase transition temperature of DPPC (16:0 PC) is 42°C and that of DMPC (14:0) is 24°C. Thus, a decrease in chain length by two carbon atoms decreases the melting temperature by 18°C. In a mixture of two or more lipids with different phase transition temperatures, the non-ideal mixing behavior of the lipids results in heterogeneous phase domains (107, 120). The miscibility of a mixture is typically represented by phase diagrams (Figure 2). Depending on the composition and temperature, the mixture can result in solid/solid, liquid/liquid, or solid/liquid, coexistence regions. Coexisting liquid-liquid phase regions are typically observed in ternary mixtures of two lipids and cholesterol. These regions are referred to as “liquid-disordered” (cholesterol-poor) and “liquid-ordered” (cholesterol-rich), and are thought to resemble lipid rafts in cell membranes. While the existence of lipid domains under physiological conditions is still debated, recent state of the art measurement techniques confirm their presence in cell membranes with sizes on the order of few tens of nanometers (29). Moreover, these domains are transient in nature, forming and disappearing on the timescales of few milliseconds (106).

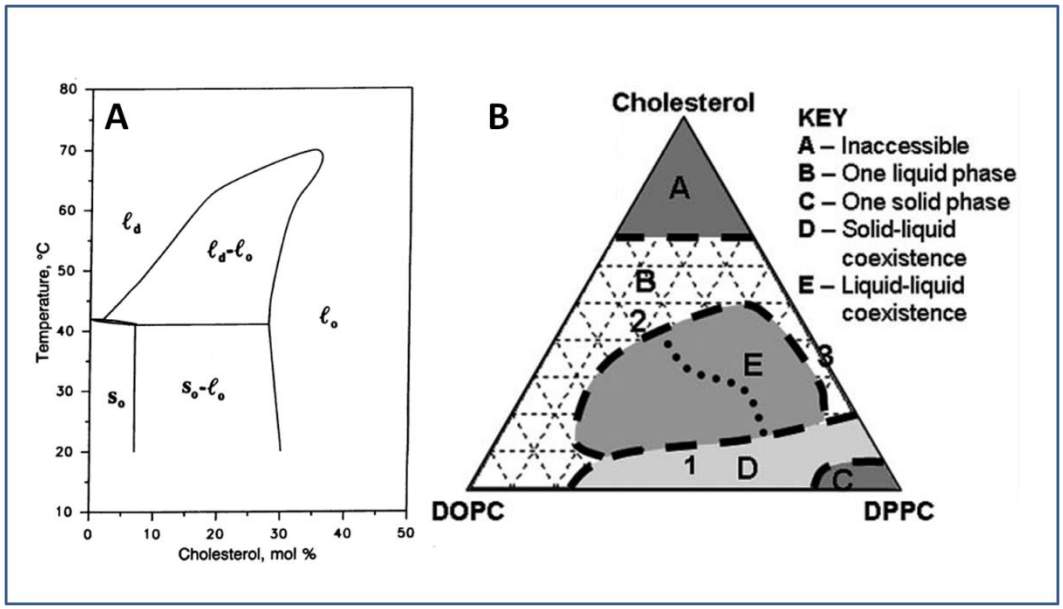

Figure 2: Phase diagram of a binary mixture of DPPC and Cholesterol (107). Phase diagram of a ternary mixture of DOPC, DPPC, and Cholesterol (120).

Giant unilamellar vesicles prepared from simple lipid mixtures (two or three components) exhibit microscopically observable phase domains, permitting their characterization under regular fluorescence microscopy (11, 13). These simplified model membrane systems closely mimic realistic biological membranes and thus provide a platform on which to build fundamental physical and chemical principles for lipid-lipid interactions. One step closer to the biological membranes is to study giant plasma membrane vesicles derived from cells that include all the membrane proteins (10). In fact, recent studies report microscopic lateral phase separation in such giant plasma membrane vesicles and several membrane proteins show preferential partitioning to these domains (10, 71).

Lipid amphiphilicity gives rise to mechanical properties.

Membranes are very flaccid materials and the bonds between molecules are dynamic and loose. So how do they resist tension? It turns out that exposure of water in the aqueous environment to the hydrophobic tails of lipids requires a significant amount of energy. The amount of mechanical energy it takes to separate lipids in the face of exposure of hydrophobic tails to water constitutes the main mechanical resistance of membranes to tension. Furthermore, moduli of lipid bilayers (bending, areal expansion, etc.) arise to a large degree from the interaction of the aqueous environment with lipids. The overall mechanics of the cell surface is also affected by the membrane-associated cytoskeleton, but this component will not be considered in this chapter.

Often membranes are considered as shells surrounding a liquid medium. But a significant result of this assumption is that the resistance to expansion with tension depends on bilayer thickness (25). However, since molecules in the membrane can rapidly rearrange in the bilayer plane in response to tension, with very little shear between molecules, the only resistance to expansion is the steric hindrance between molecules and the surface tension of the water/headgroup interface, which arises from the hydrophobic effect. When lipids are crowded together the energy penalty to bring them closer together scales as $1/a$ where a is the mean area occupied by the lipid (105). The energy penalty to move them further apart is proportional to a. If we add these two energies together, we get to total energy for a lipid, E_l, given by:

$$E_l = \gamma a + \frac{K}{a} \tag{1}$$

The proportionality constant to bring lipids apart is the surface tension, γ, since surface tension arises from the exposure of hydrocarbon tails to water. For steric repulsion, K is an undefined proportionality constant that governs the energy to bring molecules close together. It arises from steric contribution, a hydration force contribution, and an electrostatic double-layer (65). At equilibrium we would expect to be able to find an area, a_0, at which E_l is minimized such that

$$\left.\frac{dE_l}{da}\right|_{a_0} = 0 \tag{2}$$

Carrying out this derivative leads to the relation $a_o = \sqrt{\frac{K}{\gamma}}$

resulting in (after some simplifications):

$$E_l = 2\gamma a_o + \frac{\gamma}{a}(a - a_o)^2 \tag{3}$$

If we take the derivative of E_l with respect to a and solve at a=a_o we get the energy fluctuation around equilibrium. From this we conclude that the elastic energy density fluctuates by $\gamma \frac{(a-a_o)^2}{{a_o}^2}$ around a minimum area per lipid a_o (note that we have divided elastic energy by a_o to get the elastic energy density). This change in energy comes from the fact that small increments of elastic expansion of the membrane are countered by surface tension arising from the hydrophobic effect. Such tension (T)–strain relationships are governed by the compressibility modulus, such that:

$$T = K_a \frac{(a - a_o)}{a_o} \tag{4}$$

where K_a is the compressibility modulus (51). The energy density from tension, E_T/a_o of this relationship is derived from the integral of the tension over area. Therefore:

$$\frac{E_T}{a_o} = \frac{1}{2} K_a \frac{(a - a_o)^2}{{a_o}^2} \tag{5}$$

Equating the energy density from tension (equation 5) with the energy density penalty from expansion arising from exposure of hydrophobic lipid tails, $\gamma \frac{(a-a_o)^2}{{a_o}^2}$, we see that K_a =2γ for a monolayer and K_a =4γ for a bilayer. This remarkably simple yet elegant result allows us to assess the continuum property of modulus from the molecular property of surface tension.

Thus, membranes resist expansion when under stress via surface tension, and surface tension, a molecular quantity, can be related to the compressibility modulus. Because bending of a bilayer requires compression of one surface and expansion of another surface, we would expect there to be a relationship between the bending modulus and compressibility modulus. We can thus connect the bending modulus and the compressibility modulus by considering the energy it takes to deform an isotropic volume of the material. For example, the energy density of bending is:

$$E_b = \frac{K_b}{2}\left(\frac{1}{R_1} + \frac{1}{R_2}\right)^2 + \frac{K_G}{R_1 R_2} \tag{6}$$

where K_b is the bending modulus for average curvature ($1/R_1$+$1/R_2$), K_G is the bending modulus for Gaussian curvature ($1/(R_1R_2)$) (25, 63). To bend this material in one direction, R_2 goes to ∞

and therefore, $E_b = K_b/(2R_1^2)$. If we are bending a monolayer of thickness h, and we assume that the midplane of the monolayer is the neutral plane with strain = 0 at z=0, and the strain (u) increases linearly with distance z from the midplane (i.e. $u = z\cdot(u_{hg}/(h/2))$), we can show that the strain on the lipid head groups, $u_{hg} = (h/(2R_1)$. We can also compute the energy of expansion of one monolayer E_m as:

$$E_m = \frac{1}{2} K_a \langle u_m{}^2 \rangle \tag{7}$$

where $\langle u_m{}^2 \rangle$ is the average of the square of the monolayer strain. To compute this quantity, we integrate $u_m{}^2$ from z=0 to z =h/2 (where $u_m = u_{hg}$) and divide by h to get $\langle u_m{}^2 \rangle = \frac{u_{hg}{}^2}{3} = \frac{1}{12}\left(\frac{h}{R_1}\right)^2$. Substituting this result into E_m (eq 7) we get:

$$E_m = \frac{1}{24} K_a \left(\frac{h}{R_1}\right)^2 \tag{8}$$

Equating E_m (energy from expanding the monolayer) and E_b (energy of bending) we get

$$K_b = \frac{1}{12} K_a (h)^2 \tag{9}$$

This is the relation between of bending moduli and compressibility moduli for on elastic sheet of thickness h. If we have two elastic sheets, that slide past each other we can change h to h_b/2 and arrive at (for a bilayer):

$$K_b = \frac{1}{48} K_a (h_b)^2 \tag{9}$$

While we have ignored changes in thickness of the bilayer with bending, a feature that would introduce a poisson's ration, this result shows that bending rigidity is much lower than compressibility and the bending modulus depends on thickness of the bilayer. It is, of course, important to keep in mind that K_a is a true modulus that relates tension to strain. The bending modulus, K_b, has the units of energy and, since it depends on the thickness of the membrane, it is not a true material property. It can be seen that the membrane is much softer in bending than it is in tension and that the bending modulus depends on the membrane thickness, which depends on acyl chain length. In short, membranes easily fold and bend but do not easily expand. Thus we might expect that activation of proteins in the bilayer might be easier upon bending of the membrane rather than upon stretching it. If bending causes membrane thickness changes, then proteins embedded in membranes would experience hydrophobic mismatch upon membrane bending. In addition, there are proteins that prefer bent membranes. As a consequence, membrane bending fluctuations could be a significant source of protein activation and could be a mechanism of dynamic protein sorting (49).

Can stretching or bending appreciably alter hydrophobic mismatch?

Membrane-mediated protein activity can be classified into two categories: specific interactions of lipids with proteins inducing conformational changes, and non-specific interaction in which lipid bilayer physical properties modulate protein conformational changes by indirectly altering the energetic state of proteins. Various physical properties of the lipid bilayers including

viscosity, hydrophobicity, compressibility, curvature, and lateral pressure, are thought to play essential role in modulating integral membrane protein activity (66). A key property of the lipid bilayer that has a strong influence on the protein conformation is its hydrophobic thickness (4). Matching the hydrophobic thickness of the lipids to that of the embedded proteins avoids the energetic costs associated with exposing to water the hydrophobic side chains of these integral proteins (30, 61). Mismatching the hydrophobic thickness of the lipid bilayer to the protein can result a change in the lipid or protein's conformation or both (59, 95). Hydrophobic mismatch has been shown to influence the opening and closing of transmembrane stretch-activated ion channels (76). Moreover, such hydrophobic mismatch can also drive aggregation or oligomerization of the membrane proteins (17, 54, 97). Interestingly, lipid-lipid mismatch can also drive membrane segregation into domains, (7) which in turn can facilitate segregation of membrane proteins. Another well-studied property of the lipid bilayer is its fluidity (i.e. inverse of viscosity). Fluidity of the lipid bilayer can be modulated through compositional changes or through application of external mechanical forces (19, 20, 44). Though changes in fluidity cannot directly influence the activation barrier for proteins (66), it could potentially alter the kinetics of ligand-receptor interactions or protein-protein interactions in the membrane (6, 109). Nicolau et al. (89) have shown that the diffusion characteristics of raft and non-raft regions can also determine the residence time of the protein in raft regions and thus the protein concentrations in rafts. Moreover, several anesthetics and drugs are known to alter the cellular function through interactions with the plasma membrane and alteration in membrane fluidity (39).

While bilayer thickness and fluidity have been investigated for a long time, more recent studies show that other properties of the lipid bilayer such as curvature and lateral pressure profiles might also influence protein sorting and activity (43, 77). While theories for how hydrophobic mismatch induces protein conformational change tend to focus on free energy transfer, alteration of depth-dependent lateral pressure can provide a means to induce conformational changes non-uniformly along the transverse direction of the protein (22). So far, this mechanism has been investigated only theoretically or through the use of computational molecular dynamics, as lateral pressure profiles cannot be obtained experimentally. Membrane curvature is a well-observed phenomenon that is critical for membrane budding and fusion, and plays an important role in intracellular trafficking. Bilayer curvature affects lipid-protein interactions and vice versa. Lipid curvature-induced protein sorting and protein induced lipid curvature are highly interlinked phenomena (116).

To begin, the motivation for proposing that membrane thinning occurs due to curvature changes will be shown. Thinning due to curvature changes will be compared to thinning due to tension on the membrane. Thinning of the membrane from h_o to h will be determined by looking at a simplified model that calculates thickness changes from areal strain (assuming bilayer incompressibility):

$$\epsilon_a = \frac{\sigma}{Y} = \frac{(a - a_o)}{a_o} \quad = \frac{h_o}{h} - 1 \tag{10}$$

or

$$h = \frac{h_0}{\frac{\sigma}{K_a / h_0} + 1} \tag{11}$$

Note that we let the Young's modulus, $Y = K_a / h_0$.

Let us consider the shearing of a membrane by flow. Such a problem may be relevant to the effects of blood flow on vascular endothelium (21). For simplicity, it is assumed that a rectangular piece of membrane is anchored on one side with the dimensions of 10 μm by 100 μm from the top and a thickness of 4 nm (note that we have neglected the role of the glycocalyx in this example; a more thorough treatment of this type of problem can be found in (37)). In addition, it is assumed that a shear stress of 10 dynes/cm^2 (1 Pa) is applied to the surface of a membrane with a Young's modulus of 250 x 10^6 Pa (Y) (87) or K_a = 1 N/m which is the order of magnitude of the modulus of membranes with cholesterol (87). For this shear, the integrated force on the top surface stress will be 1 Pa x 1000 μm^2 yielding 10^{-9}N. This force will act along the membrane cross section of area 4 nm x 10 μm. The resulting stress (σ) in the membrane is then 0.025x10^6 Pa (force/area). Substituting this stress into equation 11 yields a decrease in membrane thickness of <0.001 nm. Thus, lateral tension from fluid flow yields an almost negligible change in membrane thickness. Whereas this example is related to shear stress on vascular endothelium, other forces on membrane from cilia, or those experienced during cell stretching may be much larger (76).

As we saw before, membranes bend more easily than they stretch. Recently, Nir Gov (40) showed that the thickness and static curvature of membranes are related by:

$$h \cong h_0 \,(1 - h_0 H + 2h_0{}^2 H^2) \qquad (12)$$

In which Gaussian curvature is assumed to be zero. Here, the mean curvature is *H*, the initial thickness of the membrane is h_0, and the final thickness is *h*. The derivation for this equation is modified from (105).

Using the above equation relating membrane thickness and curvature, we can construct the following graphs.

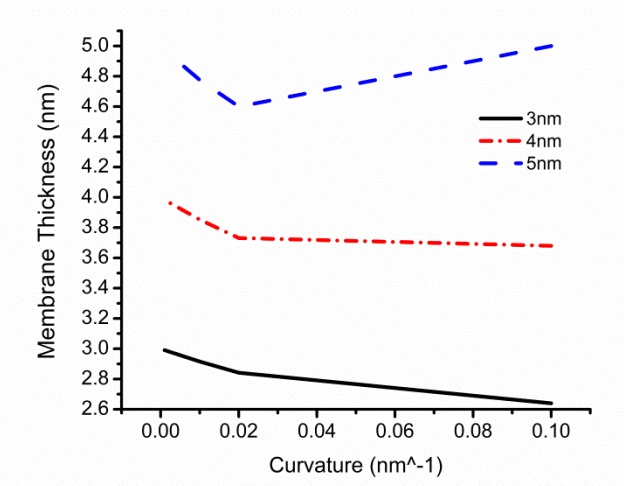

Figure 3: Membrane thickness changes with mean curvature for three different initial membrane thicknesses. The radii of curvature range from 10 nm to 1 µm.

Figure 3 illustrates that the relationship between membrane thickness and mean curvature is quadratic. The radii of curvature used to construct theses graphs range from 10 nm (very small vesicles), to 1 µm (cell scale). Hence, when the membrane is thick, curvature causes either a decrease or increase in thickness, depending on the initial curvature. With thin membranes, curvature changes tend to cause a thinning of the membrane. Thus, the starting thickness will

affect the magnitudes of the final thickness. In addition, the thicker membranes (e.g. 5 nm) will see a larger percentage change in thickness than thinner membranes (e.g. 3 nm) upon bending. Such insight may be relevant for domains that are separated due to hydrophobic mismatch arising from thickness differences. Conversely, bending can differentially change membrane thickness depends on variability in the membrane's original thickness resulting from heterogeneous lipid composition. Such an occurrence could lead to further phase separation or mixing.

We can now try to assess if the curvature-induced membrane thickness is sufficient to activate integral membrane proteins. According to (122), free energy (G_U) from hydrophobic mismatch can be quantified using the relation

$$G_U = \frac{1}{2} K_{eff} U^2 \cdot 2\pi R \tag{13}$$

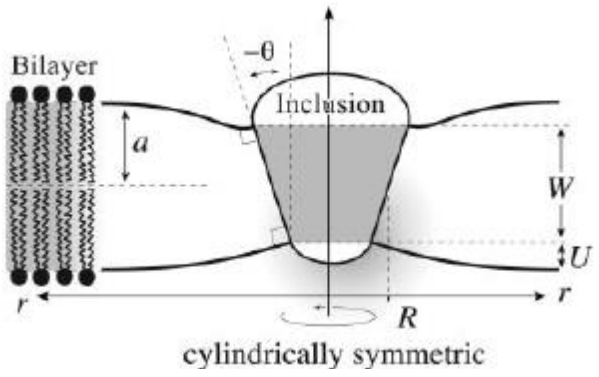

Figure 4: protein inclusion in bilayer experiencing hydrophobic mismatch (122).

Figure 4 shows a representation of the model proposed by Wiggins and Phillips and shows *R* as the radius from the center of the inclusion to the end of the mismatch region and *U* as half the hydrophobic mismatch. In the equation above, K_{eff} represents an effective elastic modulus $K_{eff} = \sqrt{2}\left(\frac{K_a{}^3 K_b}{a^6}\right)^{1/4}$. For K_a=2.33 k_BT Å^{-2} (K_a =1 N/m @ 37˚C), K_b =78 k_BT (from eq. 9), and 2a=40 Å, K_{eff} = 8.86 x 10^{-2} k_BT Å^{-3}.

In order to determine whether or not protein activation is feasible with membrane thickness changes, the elastic energy from hydrophobic mismatch was calculated using the values, K_{eff} = 8.86 x 10^{-2} k_BT·Å^{-3}, U = ½ * (hydrophobic mismatch), and R = radius of the protein inclusion. In addition, the hydrophobic mismatch was calculated using equation. (*hydrophobic mismatch*) = *h*– (*length of protein hydrophobic region*).

In order to judge whether the thinning of the membrane from bending is sufficient to provide the energy of activation for an embedded protein, we can consider the gramicidin system,

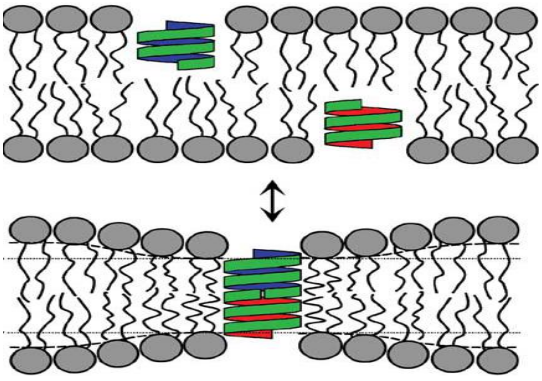

Figure 5: Gramicidin channels exist in two subunits, when inactive (top), that connect when activated (bottom) (3).

which has been used as a binary (on-off) indicator of membrane thinning. Gramicidin dimerizes under appropriate condition of membrane thickness (50, 74). Shown in Figure 5, it is an antibiotic ion channel, sensitive to univalent cations such as Na^+, H^+, and K^+, derived from *Bacillus brevis*. This tryptophan-rich protein is made up of an all single-stranded right-handed β-helical dimer that has an alternating L-D-amino acid sequence and a mass of ~4 kD. For gramicidin to activate in membranes, the two subunits undergo transmembrane dimerization. Dimerization occurs to minimize unfavorable hydrophobic-hydrophilic interactions in order to match the hydrophobic regions of the protein with the hydrophobic regions of the membrane. Stabilization of the activated molecule occurs through six hydrogen bonds between the end CO and NH groups from either subunit. In order for activation to occur, membrane deformation must take place to thin the membrane to accommodate the specific thickness of the activated channel. The membrane thickness needed for dimerization is not exactly known due to membrane undulations and fluctuations over time (3). However, estimates of the thickness are around 21.7 Å (53). Such a dimension can only be achieved through membrane thinning (3) since normal membrane hydrophobic thickness dimensions range from about 25 Å to 35 Å (14) (for a 40 Å thick bilayer in our example).

We first address the question of whether the thinning of a membrane due to curvature changes might be sufficient to be detected with Gramicidin. The length of the hydrophobic region of the Gramicidin channel is estimated to be 21.7 Å. In an example where shear forces cause a membrane to go from flat to exhibiting folds with diameters of 50 nm, the curvature would change from 0.001 nm^{-1} to 0.02 nm^{-1} and the thickness (eq. 12 and figure 3) would change from 3.73 nm to 3.98 nm (assuming a totally flat membrane is 4 nm). If we subtract 8 Å for each

leaflet headgroup region, the hydrophobic mismatch can be calculated to range from -0.4 to 2.1 Å. Therefore, it is possible that such membrane thinning could lead to gramicidin activation if the initial membrane thickness were within range. Alternatively, we can calculate the energy of hydrophobic mismatch and compare that value to the activation energy of integral membrane proteins. For a protein of hydrophobic thickness of 21.7 Å, let the radius, R, of a channel (e.g. gramicidin) be ~10 Å. If we insert these values into equation 13 to determine changes in G_U we obtain a resulting free energy change from 4 k_BT to 0.01 k_BT, for a change of ~4 k_BT. The gramicidin activation energy is 10.4 k_BT per channel (24). Therefore, although the activation energy is on the right order of magnitude, it may not be enough to activate this channel. However, this activation energy may be sufficient to activate other bilayer spanning proteins. For membranes with a low initial thickness (30 Å), their hydrophobic mismatch is small, hence the available free energy may not be sufficient to activate a gramicidin channel. For all other thicknesses, the free energy from changes in hydrophobic mismatch is either equal to or greater than the activation energy of gramicidin. Despite the many simplifications in this analysis, it can be concluded that forces that alter curvature on the cell surface, such as shear flow (108), may be sufficient to activate proteins via changes in membrane curvature and the attendant change in bilayer thickness. Further analysis is necessary to determine if the cortical spectrin or actin cytoskeleton that supports membrane in many eukaryotic cells has sufficient compliance in the face of physiological stresses, to allow the alterations in lipid bilayer curvature.

Moving from continuum mechanics to molecular dynamics

Mechanical forces modulate cell growth, differentiation, signal transduction, transport, and migration, through biochemical signaling pathways (52) which may be related to membrane molecular organization and dynamics (9, 20, 23). For example, lateral membrane tension causes conformational changes in integral membrane proteins (23), affects membrane permeability (91, 101), lipid lateral diffusion (19, 20), and organization of lipid rafts (7, 38). These effects are believed to be mediated by bilayer thickness changes that result in hydrophobic mismatch between the lipid acyl chains and transmembrane region of proteins, leading to distortion of the lipid bilayer and concomitant protein conformational changes (4, 61, 66). As we showed earlier, tension is most likely to alter membrane thickness through alterations in membrane curvature rather than lateral tension per se.

Despite the importance of lipid dynamics in cell signaling, to date the only experimental studies quantifying the relationship between lipid dynamics and force have been conducted in sheared endothelial cells (19, 20, 44) and in hair cells (81, 90). In these studies, a lipoid dye, such as 1,1'-dioctadecyl-3,3,3',3'-tetramethylindocarbocyanine perchlorate (DiI), 9-(Dicyanovinyl)-julolidine (DCVJ), or di-8-ANEPPS, was used to infer lipid dynamics from fluorescence intensity or fluorescence recovery after photobleaching (FRAP). Because these studies probed lipid dynamics indirectly and because the precise membrane tensions, at the molecular level, were unknown, there is a need to quantify directly the relationship between membrane tension and lipid dynamics.

The most prominent methods to assess lipid dynamics, including FRAP, fluorescence correlation spectroscopy (FCS), fluorescence anisotropy, and fluorescence lifetime imaging (2, 5, 42) probe membrane lipid dynamics by analyzing the dynamics of lipophyllic fluorescent dyes (e.g. DiI, 1,6-diphenyl-1,3,5-hexatriene (DPH), and Laurdan). In particular, DiI is popular because of its structural similarity to phospholipids and its ability to selectively partition into different lipid phases (gel or fluid) depending on the matching between the length of its alkyl chains and the lipid acyl chain length (92). Spectroscopic investigations employing DiI have been used to study membrane organization and dynamics (58, 92). The fluorescence lifetime of DiI depends on the accessibility to water (86) and on the viscosity of the local microenvironment (92), offering a useful tool to detect lipid rafts in cells and phase separation in model membranes. However, proper interpretation of these fluorescence measurements requires precise knowledge of location, orientation, and interactions of dye with lipids and water, which are difficult to obtain experimentally (41, 102). Examples of the utility of using molecular dynamics (MD) simulation as a tool to answer these questions include predictions of the location of drug-like small molecules in lipid bilayers along with validation by small-angle neutron scattering experiments (15, 16).

The aim of a recent computational modeling study was to determine the effects of membrane tension on mechanotransduction-related structural and dynamical properties of the bilayer (83). In addition, we wished to understand the fidelity with which DiI, a popular membrane probe, reflects lipid dynamics, so that DiI photophysics could be used as a readout for tension effects on stressed membranes. To accomplish this goal, we performed a series of atomistic molecular dynamics (MD) simulations of fluid-phase dipalmitoylphosphatidylcholine (DPPC)/DiI

bilayers under various physiological tensions. The main readouts from this study are as follows. First, we characterized the effects of tension on bilayer thickness, acyl chain packing, and leaflet interdigitation. Second, we determined the relationship between area-per-lipid and lipid lateral diffusion, and compared these results to predictions from free-area diffusion theory. Third, we compared the DiI probe dynamics to the dynamics of the native lipids, leading to an analysis of the relationship between lipid packing and fluorescence lifetime of DiI in terms of hydration and local viscosity.

Our first observation was that tension induces bilayer thinning and interleaflet interdigitation. Surface tension was estimated from the pressure tensor, as described in (31). As expected, the surface tension increased linearly with an increase in area, from -2.6 mN/m at $\alpha = 0.635$ nm^2 to 15.9 mN/m at $\alpha = 0.750$ nm^2, above which rupturing of the bilayer was observed. While this rupture tension is in good agreement with values from micropipette aspiration of lipid vesicles (ranging from 10 to 20 mN/m (101)) MD simulated rupture and experimental rupture tensions often differ because rupture/pore tension depends strongly on the loading rate, which is effectively larger in MD simulations (118). Thus within the range of tensions simulated in this study, pore formation or rupture cannot be observed in the size/time scales studied (67). Zero surface tension corresponded to $\alpha = 0.646$ nm^2, close to the experimental value of 0.64 nm^2 for DPPC (85). In addition, the area compressibility modulus calculated from the tension- area plot (31) was 105 mN/m, in good agreement with the previous simulation value of 107 mN/m for DPPC bilayer at 50°C (31). Experimentally, compressibility modulus values of 145 mN/m (64) and 234 mN/m (100) were reported for DPPC at 50°C and DMPC at room temperature, respectively. Using an identical force field to the current simulations, Lindahl *et al*. (70) reported

a simulated value of 250-300 mN/m for a larger membrane patch (1024 lipids), suggesting that the lower value in the current study is likely due to the finite-size effect. Considering the empirical nature of the force field parameters, these results indicate that the simulation methodology is sufficiently accurate in determining the microscopic and macroscopic properties of the lipid bilayer over an extended range of simulated tensions.

Bilayer thickness, defined as the distance between water and lipid density crossover points on either side of the bilayer, was directly computed from the mass density profiles (figure 6) (102). The bilayer thickness decreased linearly with increases in area-per-lipid, consistent with volume-incompressibility. The density profile of the bilayer is highly reminiscent of a confined film rather than a constant density bulk fluid – and thus changes in bilayer thickness are expected to result in structural reorientations within the bilayer (75). In support of this interpretation, it was observed that increasing the surface area resulted in a decrease of the lipid density at the headgroup region and a concurrent increase in the local density at the mid-plane of the bilayer (figure 6). This indicates increased interdigitation of the acyl chains of the opposing leaflets due to extension of the chains beyond the bilayer mid-plane. Increased interdigitation has physiological implications; for example, acyl interdigitation has been proposed to result in the formation of membrane micro-domains (64). Also, interdigitation of the acyl chains can alter the hydrophobic interactions and lateral pressure profile of the bilayer, which in turn can alter protein conformation (22, 96).

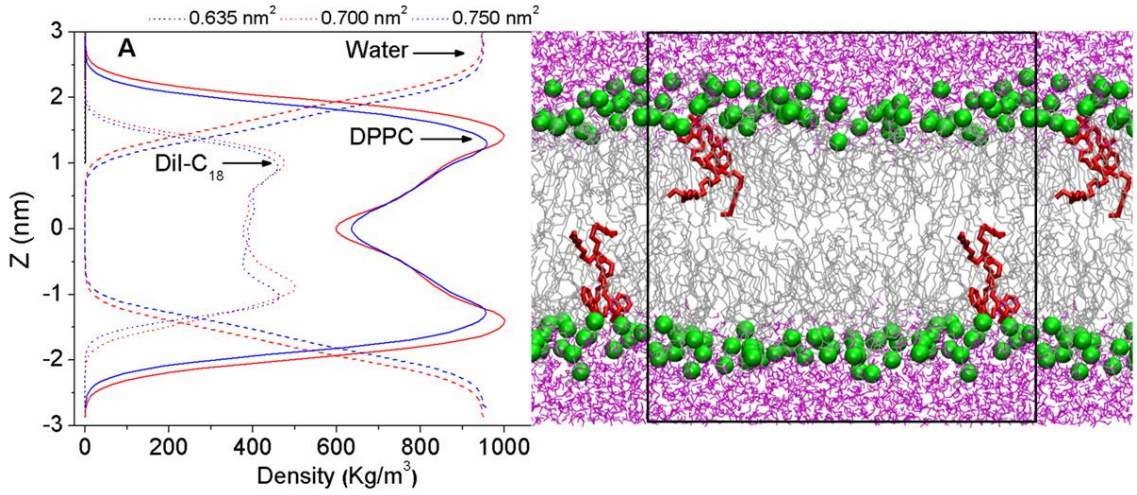

Figure 6: Mass density profiles of lipid (solid), water (dashed), and DiI-C18 (dotted) across the lipid bilayer at selected values of area-per-lipid (the center of the bilayer was set at z = 0, DiI density is at 20x for clarity). A snapshot of the simulation box is also shown (DPPC – grey, DiI – red, water – purple, and DPPC phosphorous atoms are shown in green). (83)

Moderate tension increases lipid lateral diffusion by increasing free-area, but free-area theory does not hold for large tensions. Lateral diffusion coefficients (D) were computed from the mean-squared displacement (MSD) of the center-of-mass (COM) motion of the molecules. The MSD was ensemble averaged and calculated for multiple time-origins, and D was quantified through Einstein's equation:

$$D = \lim_{t\to\infty} \frac{1}{2dt} \langle [\vec{r_i}(t+t') - \vec{r_i}(t')]^2 \rangle \qquad (15)$$

where, r_i are the *x,y* positions of the center of mass of a lipid *i* at a given time *t'* and after a time interval *t (i.e.,* at time *t+t'*); *d* is the dimensionality of the motion considered (here *d*=2 for the

in-plane lateral diffusion); the brackets denote ensemble average (over molecules and time) and also over multiple time origins *t'*. The MSDs were corrected for the COM motion of the membrane (*i.e.* removing any net leaflet translation). MSDs of DPPC at different area-per-lipid values are shown in figure 7. Simulation-measured diffusion coefficient of DPPC at α = 0.635 nm^2 was 8.1 x 10^{-12} m^2/s, which is close to the values obtained using fluorescence correlation spectroscopy (58).

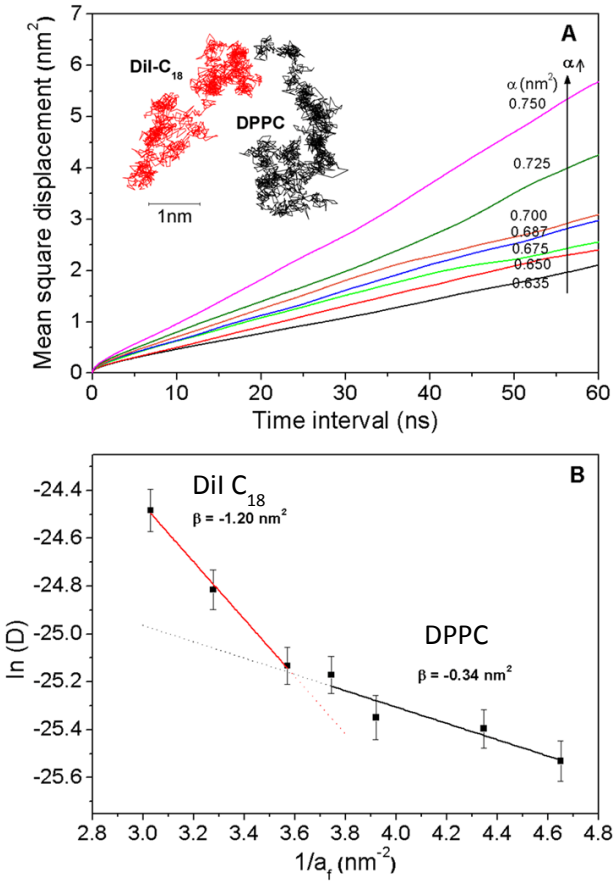

Figure 7: (A) Mean square displacements (MSD) of lipid molecules under different tensions. Representative *xy*-trajectories of DPPC and DiI molecules are shown in the inset (α = 0.635 nm^2). (B) The plot of *ln(D)* vs. $1/a_f$, where two different linear regimes were identified, represented by solid lines, with slopes *β*. Error bars represent standard errors, n = 124. (83)

Changes in lipid packing are reflected in changes in DiI diffusion and rotation. Experimentally, membrane dynamics are often assessed using measurements of dynamics of fluorescent probe molecules (2, 42, 58, 92). Such spectroscopic measurements assume that the probe molecules

faithfully reflect lipid dynamics. Interpretation of the obtained data necessitates knowledge of the microenvironment factors such as hydration and viscosity, which are dictated by the location and orientation of the chromophore.

We then found that fluorescence dynamics of DiI were sensitive to lipid packing and compared DiI dynamics to the native lipid dynamics. The lateral diffusion coefficient of DiI has been shown to be in the same range but slightly lower than that of DPPC (41). In this study, we could not test the sensitivity of long-time lateral diffusion coefficient of DiI to lipid packing due to lack of sufficient statistics; there exist only two DiI molecules in the simulation box compared to 124 DPPC molecules. Nevertheless, based on the above observations, we conclude that the lateral diffusion mechanism of DiI is similar to that of the native lipid and that tension induces increases in DiI diffusion that are quantitatively similar to lipid diffusion.

Key findings from the simulations are as follows. First, physiologically relevant tensions in the range of 0-15 mN/m caused decreases in bilayer thickness in a linear fashion consistent with volume-incompressibility. Second, tension induced a significant increase in acyl chain interdigitation and a decrease in lipid order. Third, the observed lateral diffusion coefficient of DPPC cannot be described satisfactorily using the free-area theory, across all tensions applied, due to a significant change in molecular shape and friction at high tensions. Finally, DiI has systematically lower lateral and rotational diffusion coefficients compared to DPPC, but the increase in each with tension is quantitatively similar for DiI and DPPC. Similarly, fluorescence lifetime of DiI, which depends on lipid order near the head groups, appears to be a good indicator of tension in membranes.

Experimentally, DiI sensitivity to membrane tension may be revealed in fluorescence lifetime measurements. Although the present classical molecular dynamics simulations cannot simulate fluorescence, which is a quantum mechanical process, they do enable one to assess the local physical factors that govern fluorescence. In general, fluorescence lifetime of carbocyanine chromophores is sensitive to water accessibility and to the local microviscosity. Cyanine dyes exhibit weak fluorescence in water and a dramatic increase in quantum yield upon incorporation into lipid membranes (86). Viscosity-dependent fluorescence lifetime of cyanine dyes has been shown to be related to changes in the trans-cis photoisomerization dynamics of the central methine bridge (84, 121). Moreover, Packard and Wolf have shown that fluorescence lifetime of DiI increases with an increase in order of the lipid acyl chains (92).

Thus, we present some preliminary data suggesting that tension can change the diffusion of molecules in the membrane. Giant unilamellar vesicles (>10 um) were used to assess mechanism of tension-induced reorganization by measuring changes in molecular motion of domain-sensitive fluorescent lipoid dyes using TCSPC. Figure 8 shows the relationship between tension and measured molecular dynamics in stressed membrane of uniform-composition.

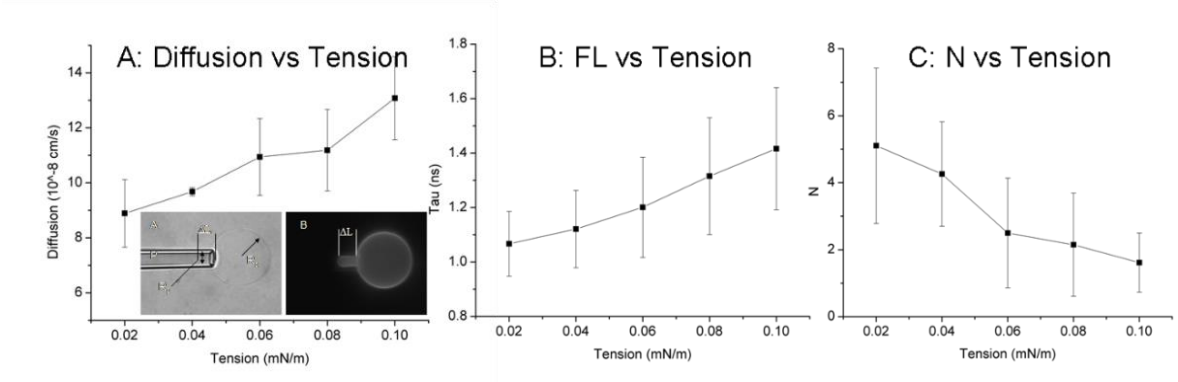

Figure 8: Membrane tension-induced: **A.** increase in diffusion coefficient **B.** Increase in fluorescence lifetime (FL) **C.** Decrease in apparent number of molecules (N) in observation volume (mean ± SD, n=4). Inset in (A) are images of aspirated vesicle.

Figure 8C, in which the number of molecules in the confocal volume decreases with tension suggests that the membrane undergoes curvature fluctuations and flattens out with increased tension. Such changes in curvature would thicken the membrane, thus decreasing the area per lipid (40). Such decreases in area per lipid is consistent with an increase in fluorescence lifetime (Figure 8B). Decreased area per lipid is expected to provide less opportunity for trans-cis isomerization of the DiI chromophore leading to an decrease in the non-radiative decay rate. Such a decrease in non-radiative decay should shorten the fluorescence lifetime, as is observed. However, if the membrane is becoming thinner, it is difficult to understand the increase in diffusion with increased tension if the main mechanism is changes in curvature. However, the apparent diffusion coefficient may increase if the path of a diffusing molecule is a flat plane rather than over a hilly terrain (40). Although more work is needed to understand this trend, it is clear that TCSPC analysis of lipoid dyes in membrane provides an unprecedented window into the dynamics of lipids in membranes under stress.

These results have potential physiological implications. For instance, hydrophobic mismatch between lipids and proteins causes opening and closing of transmembrane stretch-activated ion channels (76). Altered lipid mobility, due to force-induced changes in lipid packing, can lead to changes in protein molecular mobility and change the kinetics of enzymatic reactions that require protein complex formation (e.g. dimerization) (6, 109). Force-induced changes in lipid mobility are also associated with regulation of mitogen activated protein (MAP) kinase activity (80, 111). To explain the relationship between lipid mobility and membrane protein-mediated signaling, Nicolau *et al.* (89)[72] proposed that a local decrease in lipid viscosity, reflected in lipid mobility, temporarily corrals membrane proteins and increases their residence time and interaction kinetics leading to initiation of MAPK signaling pathways once a threshold residence time is reached (117). Studies on model membranes have demonstrated that membrane tension promotes formation of large domains from microdomains in order to minimize line tension developed at microdomain boundaries (64, 88), and there exists a critical pressure at which lipid phase separation into liquid-ordered and liquid-disordered domains is observed (60). Taken together, these studies point to changes in bilayer structure and dynamics as a mechanism of force-induced biochemical signaling.

Future research will be needed to develop a new theory for tension-diffusion relationship that takes into account frictional and molecular shape changes. The simulations described here not only provide additional quantitative insights into some of the well-studied bilayer properties (e.g. bilayer thickness, diffusion coefficient), but also lead to novel hypotheses related to membrane-mediated mechanotransduction in cells (e.g. interdigitation) that can be tested experimentally.

In addition, we tested which DiI fluorescence spectroscopic properties have potential as reporters of membrane tension effects on lipids. We observed that although DiI exhibited slower lateral and rotational diffusion compared to DPPC, its lateral and rotational diffusion increased with tension in a manner quantitatively similar to DPPC. This suggests that changes in DiI dynamics are good indicators of membrane tension. We also showed that hydration of the dye does not vary with packing, whereas the local viscosity experienced by the dye changes significantly. These results support the utility of DiI as a reporter of lipid packing and validate the use of DiI to label membrane cellular microdomains based on underlying heterogeneity in lipid order (5). Thus these findings offer new insights into the interpretation of fluorescence dynamics of DiI and lipids in lipid bilayer systems.

Experimental evidence for force-induced changes in membrane protein transport to focal adhesions

To conclude this chapter, we summarize a series of investigations intended to detect the role of the membrane in transduction of shear stress through alterations in the coalescence of lipid rafts and associated protein recruitment to focal adhesions. We first show how these levels of force are indeed sensed by the cells. We then show how focal adhesion formation is preceded by lipid raft recruitment, highlighting the role of the membrane in transport of proteins to focal adhesions, and focal adhesion activation, as evidence by talin recruitment. Finally, we show, using molecular dynamics simulations and imaging of phase separation in vesicles, how chemical additives that alter line tension in membrane control phase separation. We also provide preliminary data suggesting these same agents alter focal adhesion formation in

endothelial cells. Taken together, we propose a line of research in which membrane tension alters curvature leading to clustering of lipid-based proteins (Figure 9).

We first note that integrin ligation and clustering are major events in vascular tone regulation and shear-induced gene expression. Jalali *et al.,* showed that shear stress caused an increase in new ligand binding of β_1 integrins in and around focal adhesions (FAs) of endothelial cells (ECs) plated on fibronectin and an increase in ligand binding of β_3 integrins in ECs plated on vitronectin (56). In *ex vivo* arteriolar preparations, activation of the vitronectin receptor, $\alpha_v\beta_3$-integrin, and fibronectin receptor, $\alpha_5\beta_1$-integrin, induced coronary arteriolar dilation by stimulating endothelial production of cyclooxygenase-derived prostaglandins (48) which dilate blood vessels (21, 34). Thus integrin-matrix interactions at FAs are required to initiate the signaling pathway leading to shear stress-induced vasodilation and blood pressure regulation.

We also note that integrins are associated with rafts. Lipid rafts are 10-200 nm cholesterol- and sphingomyelin-enriched liquid-ordered (L_o) membrane domains that are involved in signaling and nucleate actin polymerization [reviewed in (69)] by concentrating phophatidylinositol 4,5 biphosphate (PIP_2) (62). FAs are cholesterol-rich microdomains, as are caveolae and rafts (99) and β_1 integrins are required for raft formation (114) and signaling through Rac-1 (98). Wang and colleagues found that Src-activation colocalized with Lyn, a raft marker (73) supporting an emerging picture of rafts as dynamic nanodomains that cluster the necessary critical mass of receptors (123) for downstream signaling of important pathways such as mitogen activated protein kinases (MAPK) (104) with time scales of formation of 20 ms and length scales of 10s of

nanometers (29). The dynamic formation and dissolution of rafts may be related to the dynamics of membrane bending and protein sorting (49).

It is believed that rafts can coalesce with force due to enhanced hydrophobic mismatch between liquid ordered (L_o) and liquid-disordered (L_d) membrane domains. Mismatch of the hydrophobic thickness of various lipids in the membrane bilayer drives aggregation of lipid domains (12) which, in turn, facilitates segregation or aggregation of membrane proteins (17, 54). Membrane tension induces raft clustering (7, 29) with a time course on the order of seconds (29). These studies demonstrate that rafts are poised to coalesce at physiological temperatures (71) or with minor alterations in the force landscape.

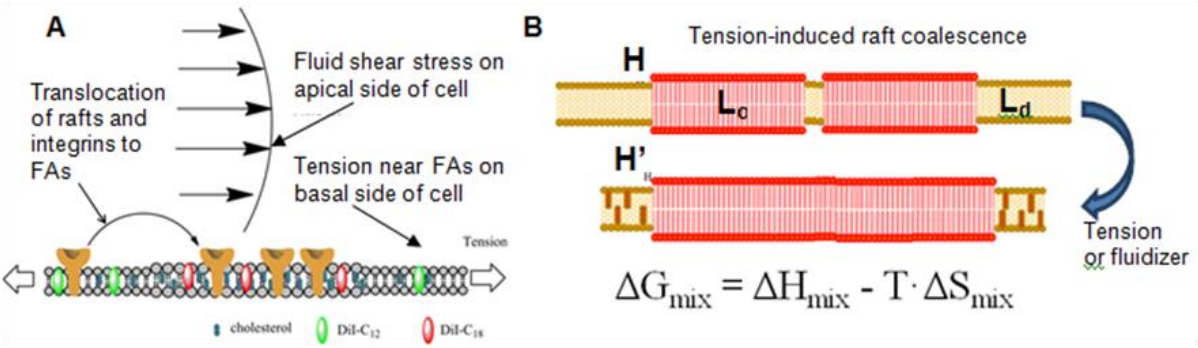

Figure 9: We hypothesize that **A** shear stress induces forces on cells that lead to increases in membrane tension near focal adhesions. This tension causes coalescence of lipid phases (**B**) and their associated integrins (**A**), by changing hydrophobic matching (from H to H') leading to focal adhesion assembly and signaling. Tension or L_d-specific amphiphiles cause coalescence of L_o. G is Gibbs free energy, H is enthalpy, S is entropy, T is temperature.

To determine if the forces experienced by sheared endothelial cells rise to sufficient magnitude for protein activation, Ferko *et al.* developed a 3-D mechanical model of an endothelial cell which predicts membrane stress distribution due to fluid flow (32, 33) (figure 10). Steady-state shear-induced stress, strain, and displacement distributions were determined from finite-

element stress analysis of a cell-specific, multicomponent elastic continuum model developed from multimodal fluorescence images of confluent endothelial cell (EC) monolayers and their nuclei. Focal adhesion locations and areas were determined from quantitative total internal reflection fluorescence microscopy and verified using green fluorescence protein-focal adhesion kinase (GFP-FAK). The model predicted that shear stress induces small heterogeneous ~100 nm deformations of the endothelial cell cytoplasm and that strain and stress were amplified 10-100 fold over apical values near focal adhesions (FAs) with magnitudes sufficient to alter domain line tension (11) and induce domain coalescence (1, 7, 11, 47, 79).

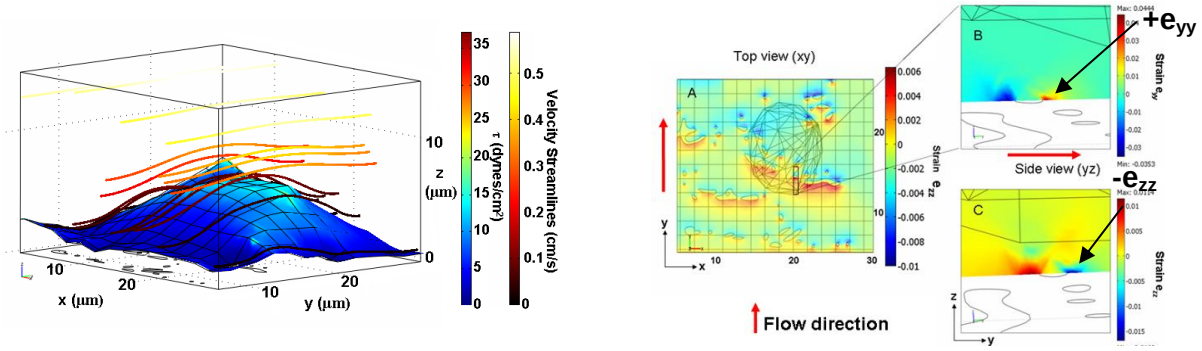

Figure 10: Shear induces stress concentrations around focal adhesions (with compression upstream and tension downstream) and in areas where there is juxtaposition of stiff organelles and soft cytoplasm (e.g. nucleus). Results suggest two mechanism of FA growth, downward deformation on the downstream side toward the ECM (negative e_{zz}) leading to new integrin ligation and lateral tension in the downstream side (positive e_{yy}) leading to raft coalescence (32).

In order to study the dynamics of lipids in membrane under stress, Gullapalli *et al.* developed a system for integrated multimodal microscopy, time resolved fluorescence, and optical-trap rheometry for single molecule mechanobiology (42) (figure 11). To enable experiments which determine the molecular basis of mechanotransduction over large time and length scales, they constructed a confocal molecular dynamics microscope. This system integrates total internal reflection fluorescence (TIRF), epifluorescence, differential interference contrast (DIC), and 3-D

deconvolution with time-correlated single photon counting (TCSPC) instrumentation and an optical trap.

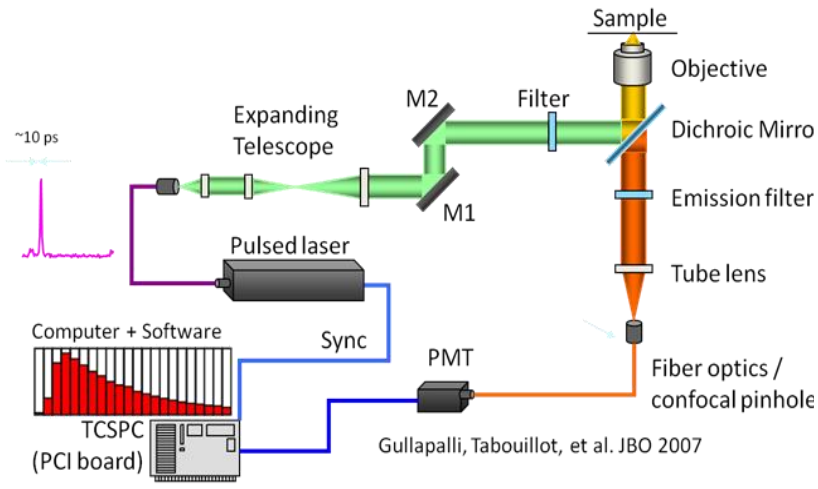

Figure 11 Confocal molecular dynamics microscope using TCSPC and pulsed laser excitation: ps pulses of laser light are directed and focused onto cells. Time stamps of laser pulse time and fluorescence photon arrival time are recorded and routed to the TCSPC electronics and analyzed for fluorescence lifetime, molecular brightness, and fluorescence correlation spectroscopy in a computer. An optical trap has been integrated into this setup with a spring constant of 13 pN/µm. (42)

Using this apparatus, Tabouillot *et al.* measured shear stress-induced modulation of single molecule diffusion, order (viscosity), and membrane surface topography (115) (figures 12 A and B): From experiments on sheared endothelial cells stained with phase domain-specific DiI-C_{18} and DiI-C_{12} they found that: (i) Shear stress induces an early and transient decrease in L_d lifetime and a later and sustained decrease in L_o lifetime. (ii) Shear stress induces a rapid increase in number of molecules in DiI-C_{12} domains and a decrease in DiI-C_{18} domains possibly due to changes in membrane curvature, and (iii) Shear stress induced an increase in lateral diffusion of DiI-C_{18} but not DiI-C_{12} (not shown). This study demonstrated that L_d and L_o domains are differentially sensitive to fluid shear stress.

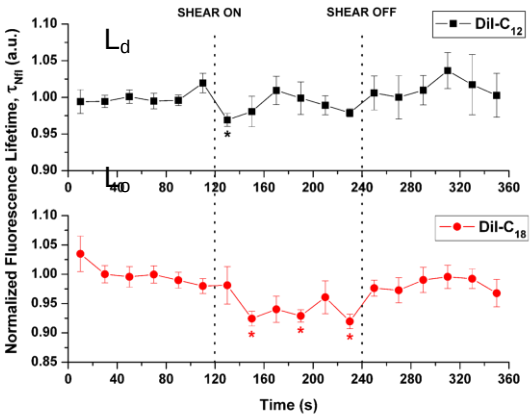

Figure 12 A: Shear induced a decrease in lifetime of DiI-C_{12} immediately at the onset of shear and for DiI-C_{18} by 40 s

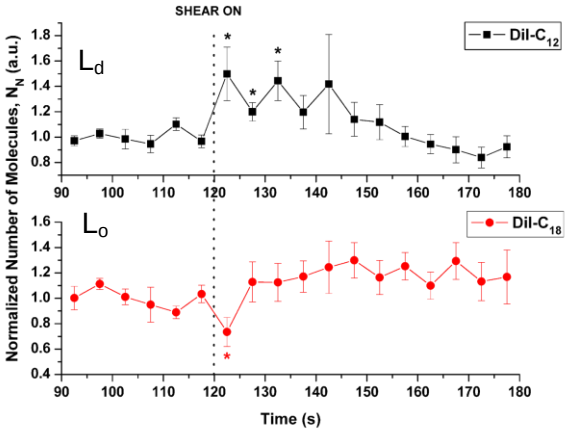

Figure 12 B: Shear induced an increase in number of molecules, for DiI-C_{12} and a decrease for C_{18}. (115)

More recently, Fuentes *et al.* measured membrane-dependent kinetics of GM-1 (rafts), integrin, and talin activation in and around nascent and mature focal adhesions. Recent studies on apical formation of focal adhesions, the effect on basal focal adhesions, and the kinetics of assembly of GM-1, actin, and talin (figure 13) suggest a model of focal adhesion assembly under force that is a complex interaction of force transmission, membrane perturbation, protein dynamics, and focal adhesion reinforcement (8, 35, 36).

In these studies, mechanical coupling between focal adhesions and GM-1 labeled rafts was discovered as were highly mobile GM-1 suggesting that there are two populations of rafts (35). Modeling the cell membrane as a 5 nm thick elastic sheet resulted in good agreement between model predictions and experimental measurements of raft displacement thus allowing the determination role of force propagation in raft and protein mobility.

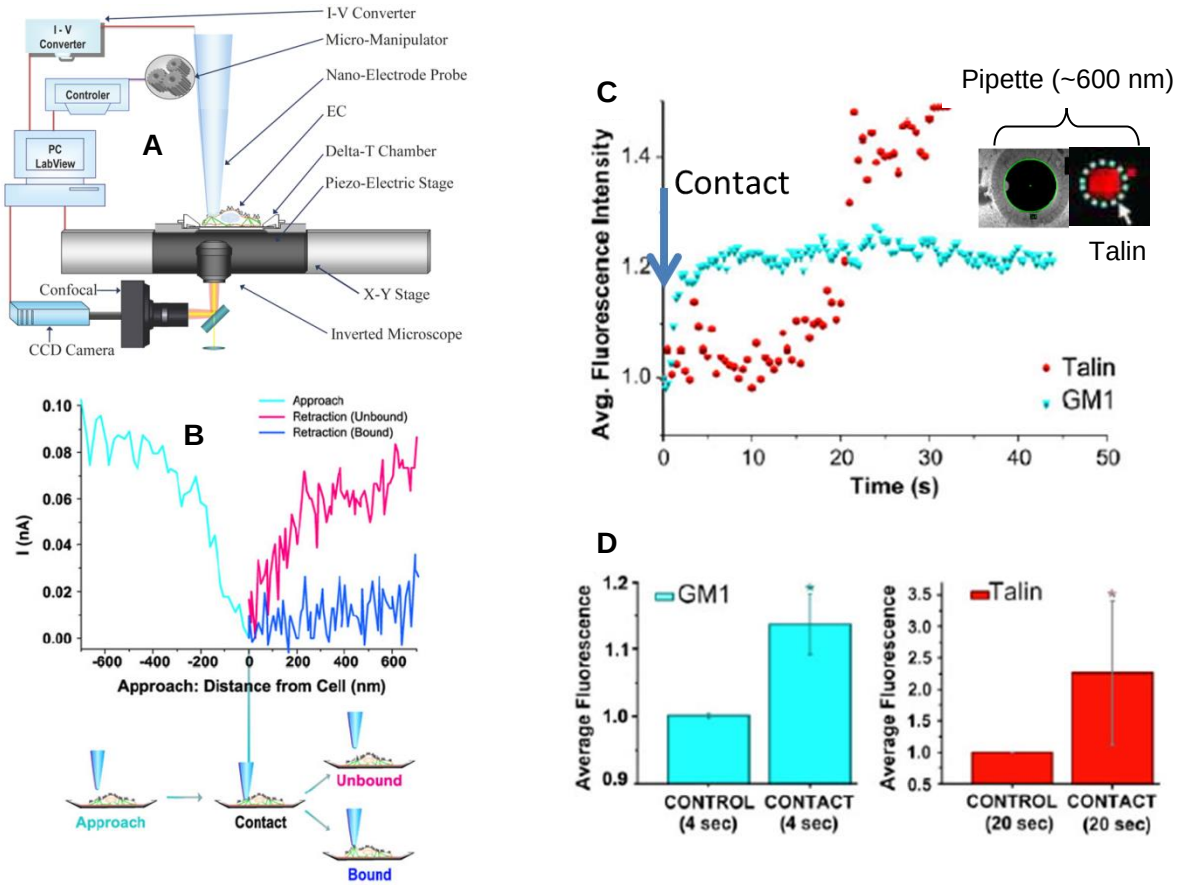

Figure 13: **A**. Pipette is functionalized with fibronectin and brought close to cell using computer control. **B**. Distance from the cell and timing of contact is determined from electronic signature. **C**. High speed confocal microscopy images at point of pipette contact with cell. **Inset**: electron micrograph of 600nm pipette tip shows conducting fiber; also, RFP talin at tip. **D**. Increase in GM-1 (membrane raft marker and talin, indicator of integrin activation. (35, 36)

In a recent study, Muddana *et al.* conducted coarsed grain molecular dynamics simulations of the additives Vitamin E, benzyl alcohol, and triton X to uncover the mechanisms by which theses additives induce domain formation or disperse them (see figure 14). In that study it was found that each of the three additives affected one phase or another by changing its thickness. Depending on the original heterogeneity of the membrane, the thickness increased domain

separation if there was an increase in mismatch of thicknesses, and decrease separation if the thickness of different lipids were brought into close agreement.

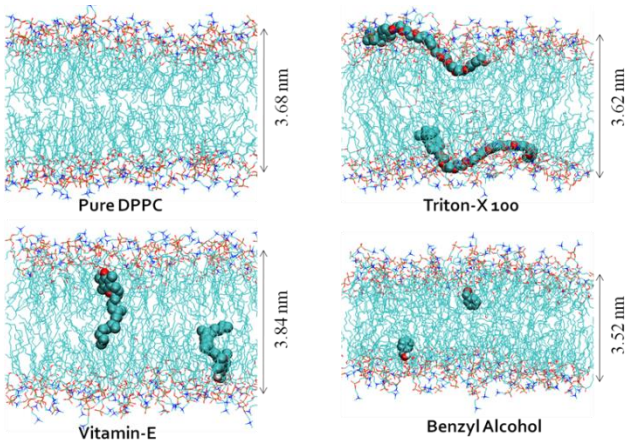

Figure 14: Left. Compared to pure DPPC bilayer, vitamin E thickens and Triton X and benzyl alcohol thin the liquid-disordered domain. With respect to figure 13, thickening L_d (red) region with Vitamin E abolishes phase separation. Thinning L_d with Triton-X and BA restores phase separation. Mechanism of phase separation is by hydrophobic mismatch between L_o and L_d phases. Thus MD simulations provide quantitative insight into effects of non-lipid amphiphiles on L_d control of phase separation. (82)

In preliminary data, we used these additives to see if they had corresponding effects on focal adhesion formation. As shown in figure 15, these additives had similar effect on focal adhesion number and size as they did on phase separation in ternary lipid mixture. Such data provides circumstantial evidence that lipid domains are important modulators of focal adhesion formation.

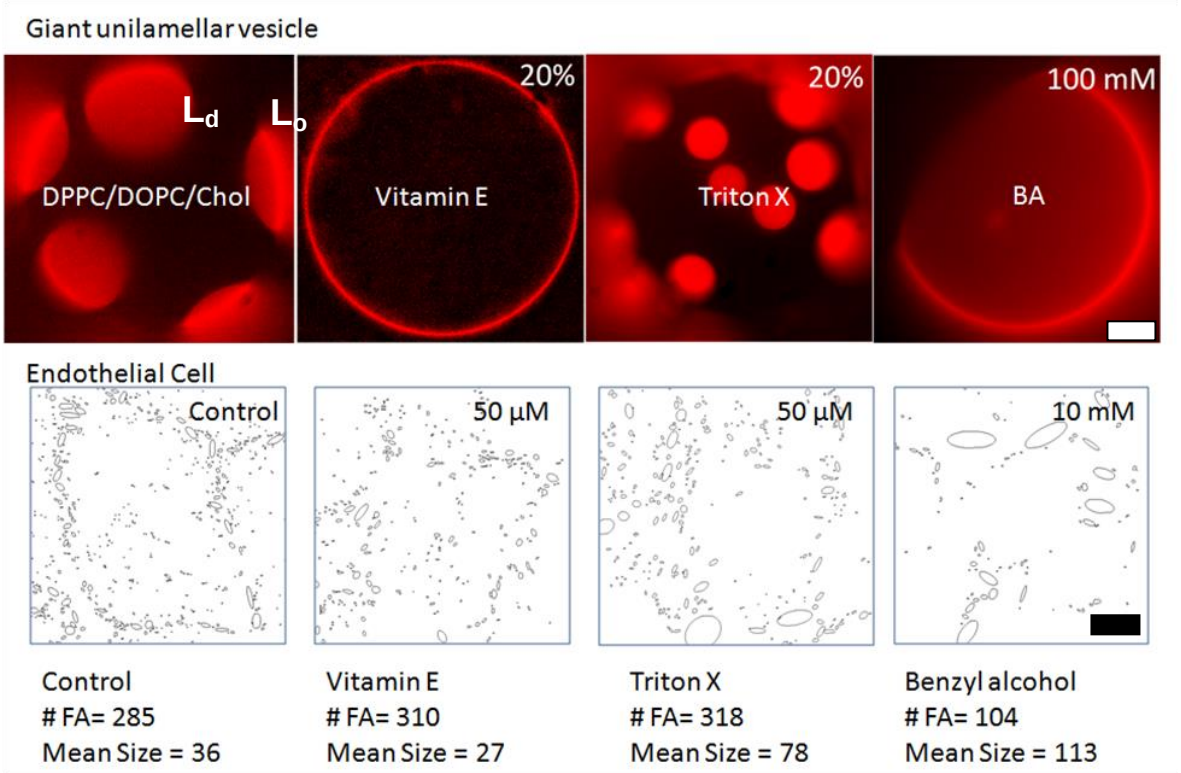

Figure 15: Top. In vesicles with L_d (red) and L_o (black) coexistence, Vitamin E (VE) disperses domains by making L_d domain match thickness of L_o domain, Triton X (TX) induces raft formation by decreasing thickness of L_d and increasing hydrophobic mismatch; Benzyl alcohol (BA) more strongly induces domain formation by further reducing L_d thickness (see figure 12 for thickness changes). (82). **Bottom**: Cells were transfected with GFP-focal adhesion kinase (FAK) and imaged under TIRF (images is of single cell were thresholded and analyzed for FA size and number). Consistent with vesicles, in cells VE increased FA number and decreased size, TX increased FA number and increased size, BA decreased FA number and increased size (sizes are in pixels). Scale bar is 10 µm. (unpublished data).

The hypothesis that tension in membrane phases plays a role in focal adhesion formation is consistent with an emerging view of focal adhesions as cholesterol-rich, liquid-ordered domains (99), much like caveolae and lipid rafts, which are stabilized by integrin attachment to the cytoskeleton and extracellular matrix. While there exist models of focal adhesion assembly in response to force, none take into account lipid control of this process, and there have not been methods to measure membrane tension or methods to delineate kinetics of assembly with and without force. These techniques are necessary to understand how lipid domains control

nascent focal adhesion formation, a prerequisite for focal adhesion-mediated mechanosensing. Despite their importance, determining membrane stresses *in vivo* (in cells) has been hampered by the membrane's complex interaction between its fluid nature and dynamic constituents (e.g. proteins and lipids) and its solid-like ability to support tension, deform, and recoil. It may now be possible to measure membrane tension using time resolved spectroscopy of DiI, a lipoid dye that intercalates into cell membrane domains in a chain-length specific manner. Second, tools based on ion-conductance spectroscopy (45) can now be used to initiate nascent focal adhesions at zero-force and to measure local kinetics of lipid raft, talin, and actin accumulation using high-speed confocal microscopy (35, 36). Third, manipulation of the hydrophobic thickness of liquid-disordered domains by non-lipid amphiphlies can be used to tune phase separation (e.g. lipid raft formation and coalescence) in model membranes (82). Combined with previous studies on force distribution in sheared and focally-adhered endothelial cells it may now be possible to uncover the relationship between force and membrane control of focal adhesion assembly and attendant signaling. Such studies may uncovered the nature of lipid control of focal adhesion function, and identify the lipid bilayer as a new target for biophysical regulation of mechanotransduction.

Bibliography

1. **Akimov SA, Kuzmin PI, Zimmerberg J, Cohen FS**. Lateral tension increases the line tension between two domains in a lipid bilayer membrane. *Physical review. E, Statistical, nonlinear, and soft matter physics* 75: 011919, 2007.

2. **De Almeida RFM, Loura LMS, Prieto M**. Membrane lipid domains and rafts: current applications of fluorescence lifetime spectroscopy and imaging. *Chemistry and physics of lipids* 157: 61–77, 2009.

3. **Andersen OS, Koeppe RE, Roux B**. Gramicidin channels. *IEEE transactions on nanobioscience* 4: 10–20, 2005.

4. **Andersen OS, Koeppe RE**. Bilayer thickness and membrane protein function: an energetic perspective. *Annual review of biophysics and biomolecular structure* 36: 107–30, 2007.

5. **Ariola FS, Li Z, Cornejo C, Bittman R, Heikal AA**. Membrane fluidity and lipid order in ternary giant unilamellar vesicles using a new bodipy-cholesterol derivative. *Biophysical journal* 96: 2696–708, 2009.

6. **Axelrod D**. Lateral motion of membrane proteins and biological function. *The Journal of Membrane Biology* 75: 1–10, 1983.

7. **Ayuyan AG, Cohen FS**. Raft composition at physiological temperature and pH in the absence of detergents. *Biophysical journal* 94: 2654–2666, 2008.

8. **Bae C, Butler PJ**. Automated single-cell electroporation. *BioTechniques* 41: 399–402, 2006.

9. **Bao X, Lu C, Frangos J a**. Mechanism of temporal gradients in shear-induced ERK1/2 activation and proliferation in endothelial cells. *American journal of physiology. Heart and circulatory physiology* 281: H22–9, 2001.

10. **Baumgart T, Hammond AT, Sengupta P, Hess ST, Holowka DA, Baird BA, Webb WW**. Large-scale fluid/fluid phase separation of proteins and lipids in giant plasma membrane vesicles. *Proceedings of the National Academy of Sciences of the United States of America* 104: 3165–70, 2007.

11. **Baumgart T, Hess ST, Webb WW**. Imaging coexisting fluid domains in biomembrane models coupling curvature and line tension. *Nature* 425: 821–824, 2003.

12. **Baumgart T, Hess ST, Webb WW**. Imaging coexisting fluid domains in biomembrane models coupling curvature and line tension. *Nature* 425: 821–824, 2003.

13. **Baumgart T, Hunt G, Farkas ER, Webb WW, Feigenson GW**. Fluorescence probe partitioning between Lo/Ld phases in lipid membranes. *Biochimica et biophysica acta* 1768: 2182–94, 2007.

14. **Boal DH**. *Mechanics of the Cell*. Cambridge University Press, 2002.

15. **Boggara MB, Krishnamoorti R**. Partitioning of nonsteroidal antiinflammatory drugs in lipid membranes: a molecular dynamics simulation study. *Biophysical journal* 98: 586–95, 2010.

16. **Boggara MB, Krishnamoorti R**. Small-angle neutron scattering studies of phospholipid-NSAID adducts. *Langmuir : the ACS journal of surfaces and colloids* 26: 5734–45, 2010.

17. **Botelho AV, Huber T, Sakmar TP, Brown MF**. Curvature and hydrophobic forces drive oligomerization and modulate activity of rhodopsin in membranes. *Biophysical journal* 91: 4464–4477, 2006.

18. **Burger K, Gimpl G, Fahrenholz F**. Regulation of receptor function by cholesterol. *Cellular and molecular life sciences : CMLS* 57: 1577–92, 2000.

19. **Butler PJ, Norwich G, Weinbaum S, Chien S**. Shear stress induces a time- and position-dependent increase in endothelial cell membrane fluidity. *American Journal of Physiology. Cell physiology* 280: C962–C969, 2001.

20. **Butler PJ, Tsou T-CC, Li JY-S, Usami S, Chien S**. Rate sensitivity of shear-induced changes in the lateral diffusion of endothelial cell membrane lipids: a role for membrane perturbation in shear-induced MAPK activation. *FASEB journal : official publication of the Federation of American Societies for Experimental Biology* 16: 216–8, 2002.

21. **Butler PJ, Weinbaum S, Chien S, Lemons DE**. Endothelium-dependent, shear-induced vasodilation is rate-sensitive. *Microcirculation (New York, N.Y. : 1994)* 7: 53–65, 2000.

22. **Cantor RS**. Lateral Pressures in Cell Membranes: A Mechanism for Modulation of Protein Function. *The Journal of Physical Chemistry B* 101: 1723–1725, 1997.

23. **Chachisvilis M, Zhang Y-L, Frangos JA**. G protein-coupled receptors sense fluid shear stress in endothelial cells. *Proceedings of the National Academy of Sciences of the United States of America* 103: 15463–8, 2006.

24. **Chernyshev A, Cukierman S**. Thermodynamic view of activation energies of proton transfer in various gramicidin A channels. *Biophysical journal* 82: 182–92, 2002.

25. **Deserno M**. Fluid lipid membranes – a primer. http://www.cmu.edu/biolphys/deserno/pdf/membrane_theory.pdf.

26. **Devaux PF, Morris R**. Transmembrane asymmetry and lateral domains in biological membranes. *Traffic (Copenhagen, Denmark)* 5: 241–6, 2004.

27. **Dopico AM, Bukiya AN, Singh AK**. Large conductance, calcium- and voltage-gated potassium (BK) channels: regulation by cholesterol. *Pharmacology & therapeutics* 135: 133–50, 2012.

28. **Edidin M**. Lipids on the frontier: a century of cell-membrane bilayers. *Nature reviews. Molecular cell biology* 4: 414–8, 2003.

29. **Eggeling C, Ringemann C, Medda R, Schwarzmann G, Sandhoff K, Polyakova S, Belov VN, Hein B, von Middendorff C, Schönle A, Hell SW, Schonle A**. Direct observation of the nanoscale dynamics of membrane lipids in a living cell. *Nature* 457: 1159–U121, 2009.

30. **Fattal DR, Ben-Shaul A**. A molecular model for lipid-protein interaction in membranes: the role of hydrophobic mismatch. *Biophysical journal* 65: 1795–809, 1993.

31. **Feller SE, Pastor RW**. Constant surface tension simulations of lipid bilayers: The sensitivity of surface areas and compressibilities. *The Journal of Chemical Physics* 111: 1281, 1999.

32. **Ferko MC, Bhatnagar A, Garcia MB, Butler PJ**. Finite-element stress analysis of a multicomponent model of sheared and focally-adhered endothelial cells. *Annals of Biomedical Engineering* 35: 208–23, 2007.

33. **Ferko MC, Patterson BW, Butler PJ**. High-resolution solid modeling of biological samples imaged with 3D fluorescence microscopy. *Microscopy research and technique* 69: 648–655, 2006.

34. **Frame MD, Rivers RJ, Altland O, Cameron S**. Mechanisms initiating integrin-stimulated flow recruitment in arteriolar networks. *Journal of applied physiology: respiratory, environmental and exercise physiology* 102: 2279–2287, 2007.

35. **Fuentes DE, Bae C, Butler PJ**. Focal Adhesion Induction at the Tip of a Functionalized Nanoelectrode. *Cellular and molecular bioengineering* 4: 616–626, 2011.

36. **Fuentes DE, Butler PJ**. Coordinated Mechanosensitivity of Membrane Rafts and Focal Adhesions. *Cellular and Molecular Bioengineering* 5: 143–154, 2012.

37. **Fung YC, Liu SQ**. Elementary mechanics of the endothelium of blood vessels. *Journal of biomechanical engineering* 115: 1–12, 1993.

38. **Garcia-Saez AJ, Chiantia S, Schwille P**. Effect of line tension on the lateral organization of lipid membranes. *The Journal of biological chemistry* 282: 33537–33544, 2007.

39. **Goldstein DB**. The Effects of Drugs on Membrane Fluidity. *Annual Review of Pharmacology and Toxicology* 24: 43–64, 1984.

40. **Gov N**. Diffusion in curved fluid membranes. *Physical Review E* 73: 041918, 2006.

41. **Gullapalli RR, Demirel MC, Butler PJ**. Molecular dynamics simulations of DiI-C18(3) in a DPPC lipid bilayer. *Physical chemistry chemical physics : PCCP* 10: 3548–60, 2008.

42. **Gullapalli RR, Tabouillot T, Mathura R, Dangaria JH, Butler PJ**. Integrated multimodal microscopy, time-resolved fluorescence, and optical-trap rheometry: toward single molecule mechanobiology. *Journal of biomedical optics* 12: 014012, 2007.

43. **Gullingsrud J, Schulten K**. Lipid bilayer pressure profiles and mechanosensitive channel gating. *Biophysical journal* 86: 3496–509, 2004.

44. **Haidekker MA, L'Heureux N, Frangos JA**. Fluid shear stress increases membrane fluidity in endothelial cells: a study with DCVJ fluorescence. *American journal of physiology. Heart and circulatory physiology* 278: H1401–6, 2000.

45. **Hansma PK, Drake B, Marti O, Gould SA, Prater CB**. The scanning ion-conductance microscope. *Science* 243: 641–643, 1989.

46. **Hanson MA, Cherezov V, Griffith MT, Roth CB, Jaakola V-P, Chien EYT, Velasquez J, Kuhn P, Stevens RC**. A specific cholesterol binding site is established by the 2.8 A structure of the human beta2-adrenergic receptor. *Structure (London, England : 1993)* 16: 897–905, 2008.

47. **Heberle FA, Petruzielo RS, Pan J, Drazba P, Kučerka N, Standaert RF, Feigenson GW, Katsaras J**. Bilayer thickness mismatch controls domain size in model membranes. *Journal of the American Chemical Society* 135: 6853–9, 2013.

48. **Hein TW, Platts SH, Waitkus-Edwards KR, Kuo L, Mousa SA, Meininger GA**. Integrin-binding peptides containing RGD produce coronary arteriolar dilation via cyclooxygenase

activation. *American Journal of Physiology. Heart and Circulatory Physiology* 281: H2378–H2384, 2001.

49. **Heinrich M, Tian A, Esposito C, Baumgart T**. Dynamic sorting of lipids and proteins in membrane tubes with a moving phase boundary. *Proceedings of the National Academy of Sciences of the United States of America* 107: 7208–7213, 2010.

50. **Helfrich P, Jakobsson E**. Calculation of deformation energies and conformations in lipid membranes containing gramicidin channels. *Biophysical journal* 57: 1075–84, 1990.

51. **Helfrich W**. Elastic properties of lipid bilayers: theory and possible experiments. *Z. naturforsch* 28: 693–703, 1973.

52. **Huang H, Kamm RD, Lee RT**. Cell mechanics and mechanotransduction: pathways, probes, and physiology. *American journal of physiology. Cell physiology* 287: C1–11, 2004.

53. **Huang HW**. Deformation free energy of bilayer membrane and its effect on gramicidin channel lifetime. *Biophysical journal* 50: 1061–70, 1986.

54. **Huber T, Periole X, Marrink SJ, Sakmar TP**. G protein-coupled receptors self-assemble in dynamics simulations of model bilayers. *Biophysical journal* 129: 10126–10132, 2007.

55. **Jacobson K, Mouritsen OG, Anderson RGW**. Lipid rafts: at a crossroad between cell biology and physics. *Nature cell biology* 9: 7–14, 2007.

56. **Jalali S, del Pozo MA, Chen K, Miao H, Li Y, Schwartz MA, Shyy JY, Chien S**. Integrin-mediated mechanotransduction requires its dynamic interaction with specific extracellular matrix (ECM) ligands. *Proceedings of the National Academy of Sciences of the United States of America* 98: 1042–1046, 2001.

57. **Jones OT, McNamee MG**. Annular and nonannular binding sites for cholesterol associated with the nicotinic acetylcholine receptor. *Biochemistry* 27: 2364–74, 1988.

58. **Kahya N, Scherfeld D, Bacia K, Schwille P**. Lipid domain formation and dynamics in giant unilamellar vesicles explored by fluorescence correlation spectroscopy. *Journal of structural biology* 147: 77–89, 2004.

59. **Kandasamy SK, Larson RG**. Molecular dynamics simulations of model trans-membrane peptides in lipid bilayers: a systematic investigation of hydrophobic mismatch. *Biophysical journal* 90: 2326–43, 2006.

60. **Keller SL, Anderson TG, McConnell HM**. Miscibility critical pressures in monolayers of ternary lipid mixtures. *Biophysical journal* 79: 2033–42, 2000.

61. **Killian JA**. Hydrophobic mismatch between proteins and lipids in membranes. *Biochimica et biophysica acta* 1376: 401–15, 1998.

62. **Kwik J, Boyle S, Fooksman D, Margolis L, Sheetz MP, Edidin M**. Membrane cholesterol, lateral mobility, and the phosphatidylinositol 4,5-bisphosphate-dependent organization of cell actin. *Proceedings of the National Academy of Sciences of the United States of America* 100: 13964–13969, 2003.

63. **Landau LD, Pitaevskii LP, Lifshitz EM, Kosevich AM**. *Theory of Elasticity, Third Edition: Volume 7 (Theoretical Physics)*. Butterworth-Heinemann, 1986.

64. **Lazar T**. The structure of biological membranes (2nd edn) P. Yeagle (ed.), CRC Press, 540 pp., ISBN 0-8493-1403-8 (2004). *Cell Biochemistry and Function* 23: 294–295, 2005.

65. **Leckband D, Israelachvili J**. Intermolecular forces in biology. *Quarterly reviews of biophysics* 34: 105–267, 2001.

66. **Lee AG**. Lipid-protein interactions in biological membranes: a structural perspective. *Biochimica et Biophysica Acta-Biomembranes* 1612: 1–40, 2003.

67. **Leontiadou H, Mark AE, Marrink SJ**. Molecular dynamics simulations of hydrophilic pores in lipid bilayers. *Biophysical journal* 86: 2156–64, 2004.

68. **Levitan I, Christian AE, Tulenko TN, Rothblat GH**. Membrane cholesterol content modulates activation of volume-regulated anion current in bovine endothelial cells. *The Journal of general physiology* 115: 405–16, 2000.

69. **Levitan I, Gooch KJ**. Lipid rafts in membrane-cytoskeleton interactions and control of cellular biomechanics: actions of oxLDL. *Antioxidants & Redox Signalling* 9: 1519–1534, 2007.

70. **Lindahl E, Edholm O**. Mesoscopic undulations and thickness fluctuations in lipid bilayers from molecular dynamics simulations. *Biophysical journal* 79: 426–33, 2000.

71. **Lingwood D, Ries J, Schwille P, Simons K**. Plasma membranes are poised for activation of raft phase coalescence at physiological temperature. *Proceedings of the National Academy of Sciences of the United States of America* 105: 10005–10010, 2008.

72. **Lipowsky R, Sackmann E**. *Structure and dynamics of membranes: from cells to vesicles*. 1995.

73. **Lu S, Ouyang M, Seong J, Zhang J, Chien S, Wang Y**. The spatiotemporal pattern of Src activation at lipid rafts revealed by diffusion-corrected FRET imaging. *PLoS.Comput.Biol.* 4: e1000127, 2008.

74. **Lundbaek JA, Collingwood SA, Ingólfsson HI, Kapoor R, Andersen OS**. Lipid bilayer regulation of membrane protein function: gramicidin channels as molecular force probes. *Journal of the Royal Society, Interface / the Royal Society* 7: 373–95, 2010.

75. **Manias E, Hadziioannou G, ten Brinke G**. Inhomogeneities in Sheared Ultrathin Lubricating Films. *Langmuir* 12: 4587–4593, 1996.

76. **Martinac B**. Mechanosensitive ion channels: molecules of mechanotransduction. *Journal of cell science* 117: 2449–60, 2004.

77. **McMahon HT, Gallop JL**. Membrane curvature and mechanisms of dynamic cell membrane remodelling. *Nature* 438: 590–6, 2005.

78. **Van Meer G, Voelker DR, Feigenson GW**. Membrane lipids: where they are and how they behave. *Nature reviews. Molecular cell biology* 9: 112–24, 2008.

79. **Méléard P, Bagatolli L a, Pott T**. Giant unilamellar vesicle electroformation from lipid mixtures to native membranes under physiological conditions. *Methods in enzymology* 465: 161–76, 2009.

80. **Mollinedo F, de la Iglesia-Vicente J, Gajate C, Estella-Hermoso de Mendoza A, Villa-Pulgarin JA, Campanero MA, Blanco-Prieto MJ**. Lipid raft-targeted therapy in multiple myeloma. *Oncogene* 29: 3748–57, 2010.

81. **De Monvel JB, Brownell WE, Ulfendahl M**. Lateral diffusion anisotropy and membrane lipid/skeleton interaction in outer hair cells. *Biophysical journal* 91: 364–81, 2006.

82. **Muddana HS, Chiang HH, Butler PJ**. Tuning membrane phase separation using nonlipid amphiphiles. *Biophysical journal* 102: 489–97, 2012.

83. **Muddana HS, Gullapalli RR, Manias E, Butler PJ, E M**. Atomistic simulation of lipid and DiI dynamics in membrane bilayers under tension. *Physical chemistry chemical physics : PCCP* 13: 1368–78, 2011.

84. **Muddana HS, Morgan TT, Adair JH, Butler PJ**. Photophysics of Cy3-encapsulated calcium phosphate nanoparticles. *Nano letters* 9: 1559–66, 2009.

85. **Nagle JF, Tristram-Nagle S**. Structure of lipid bilayers. *Biochimica et Biophysica Acta-Reviews on Biomembranes* 1469: 159–195, 2000.

86. **Nakashima N, Kunitake T**. Drastic fluorescence enhancement of cyanine dyes bound to synthetic bilayer membranes. Its high sensitivity to the chemical structure and the physical state of the membrane. *Journal of the American Chemical Society* 104: 4261–4262, 1982.

87. **Needham D, Nunn RS**. Elastic deformation and failure of lipid bilayer membranes containing cholesterol. *Biophysical journal* 58: 997–1009, 1990.

88. **Nelson DL**. *Lehninger Principles of Biochemistry*. W.H. Freeman & Company, 2008.

89. **Nicolau D V, Burrage K, Parton RG, Hancock JF**. Identifying optimal lipid raft characteristics required to promote nanoscale protein-protein interactions on the plasma membrane. *Molecular and cellular biology* 26: 313–23, 2006.

90. **Oghalai JS, Zhao HB, Kutz JW, Brownell WE**. Voltage- and tension-dependent lipid mobility in the outer hair cell plasma membrane. *Science (New York, N.Y.)* 287: 658–61, 2000.

91. **Olbrich K, Rawicz W, Needham D, Evans E**. Water permeability and mechanical strength of polyunsaturated lipid bilayers. *Biophysical journal* 79: 321–7, 2000.

92. **Packard BS, Wolf DE**. Fluorescence lifetimes of carbocyanine lipid analogues in phospholipid bilayers. *Biochemistry* 24: 5176–81, 1985.

93. **Paila YD, Chattopadhyay A**. The function of G-protein coupled receptors and membrane cholesterol: specific or general interaction? *Glycoconjugate journal* 26: 711–720, 2009.

94. **Paila YD, Tiwari S, Chattopadhyay A**. Are specific nonannular cholesterol binding sites present in G-protein coupled receptors? *Biochimica et biophysica acta* 1788: 295–302, 2009.

95. **Park SH, Opella SJ**. Tilt angle of a trans-membrane helix is determined by hydrophobic mismatch. *Journal of molecular biology* 350: 310–8, 2005.

96. **Patra M**. Lateral pressure profiles in cholesterol-DPPC bilayers. *European biophysics journal : EBJ* 35: 79–88, 2005.

97. **Periole X, Huber T, Marrink S-JJ, Sakmar TP**. G protein-coupled receptors self-assemble in dynamics simulations of model bilayers. *Biophysical journal* 129: 10126–32, 2007.

98. **Del Pozo MA, Alderson NB, Kiosses WB, Chiang HH, Anderson RG, Schwartz MA**. Integrins regulate Rac targeting by internalization of membrane domains. *Science* 303: 839–842, 2004.

99. **Del Pozo MA, Schwartz MA**. Rac, membrane heterogeneity, caveolin and regulation of growth by integrins. *Trends in cell biology* 17: 246–250, 2007.

100. **Rawicz W, Olbrich KC, McIntosh T, Needham D, Evans E**. Effect of chain length and unsaturation on elasticity of lipid bilayers. *Biophysical journal* 79: 328–39, 2000.

101. **Rawicz W, Smith BA, McIntosh TJ, Simon SA, Evans E**. Elasticity, strength, and water permeability of bilayers that contain raft microdomain-forming lipids. *Biophysical journal* 94: 4725–36, 2008.

102. **Repáková J, Čapková P, Holopainen JM, Vattulainen I**. Distribution, Orientation, and Dynamics of DPH Probes in DPPC Bilayer. *The Journal of Physical Chemistry B* 108: 13438–13448, 2004.

103. **Romanenko VG, Rothblat GH, Levitan I**. Sensitivity of volume-regulated anion current to cholesterol structural analogues. *The Journal of general physiology* 123: 77–87, 2004.

104. **Rotblat B, Belanis L, Liang H, Haklai R, Elad-Zefadia G, Hancock JF, Kloog Y, Plowman SJ**. H-Ras nanocluster stability regulates the magnitude of MAPK signal output. *PLoS.One.* 5, 2010.

105. **Safran SA**. Statistical Thermodynamics of Surfaces, Interfaces, and Membranes. Addison-Wesley Longman, Incorporated. 270, 1994.

106. **Sahl SJ, Leutenegger M, Hilbert M, Hell SW, Eggeling C**. Fast molecular tracking maps nanoscale dynamics of plasma membrane lipids. *Proceedings of the National Academy of Sciences of the United States of America* 107: 6829–34, 2010.

107. **Sankaram MB, Thompson TE**. Cholesterol-induced fluid-phase immiscibility in membranes. *Proceedings of the National Academy of Sciences of the United States of America* 88: 8686–90, 1991.

108. **Schmid-Schönbein GW, Kosawada T, Skalak R, Chien S**. Membrane model of endothelial cells and leukocytes. A proposal for the origin of a cortical stress. *Journal of biomechanical engineering* 117: 171–8, 1995.

109. **Schreiber G**. Kinetic studies of protein–protein interactions. *Current Opinion in Structural Biology* 12: 41–47, 2002.

110. **Simons K, Toomre D**. Lipid rafts and signal transduction. *Nature reviews. Molecular cell biology* 1: 31–9, 2000.

111. **Singer SJ, Nicolson GL**. The fluid mosaic model of the structure of cell membranes. *Science (New York, N.Y.)* 175: 720–31, 1972.

112. **Singh DK, Rosenhouse-Dantsker A, Nichols CG, Enkvetchakul D, Levitan I**. Direct regulation of prokaryotic Kir channel by cholesterol. *The Journal of biological chemistry* 284: 30727–36, 2009.

113. **Singh DK, Shentu T-P, Enkvetchakul D, Levitan I**. Cholesterol regulates prokaryotic Kir channel by direct binding to channel protein. *Biochimica et biophysica acta* 1808: 2527–33, 2011.

114. **Singh RD, Marks DL, Holicky EL, Wheatley CL, Kaptzan T, Sato SB, Kobayashi T, Ling K, Pagano RE**. Gangliosides and beta1-integrin are required for caveolae and membrane domains. *Traffic (Copenhagen, Denmark)* 11: 348–360, 2010.

115. **Tabouillot T, Muddana HS, Butler PJ**. Endothelial Cell Membrane Sensitivity to Shear Stress is Lipid Domain Dependent. *Cellular and molecular bioengineering* 4: 169–181, 2011.

116. **Tian A, Baumgart T**. Sorting of lipids and proteins in membrane curvature gradients. *Biophysical journal* 96: 2676–2688, 2009.

117. **Tian T, Harding A, Inder K, Plowman S, Parton RG, Hancock JF**. Plasma membrane nanoswitches generate high-fidelity Ras signal transduction. *Nature cell biology* 9: 905–14, 2007.

118. **Tieleman DP, Leontiadou H, Mark AE, Marrink S-J**. Simulation of pore formation in lipid bilayers by mechanical stress and electric fields. *Journal of the American Chemical Society* 125: 6382–3, 2003.

119. **Tokumasu F, Jin AJ, Feigenson GW, Dvorak JA**. Nanoscopic lipid domain dynamics revealed by atomic force microscopy. *Biophysical journal* 84: 2609–18, 2003.

120. **Veatch SL, Keller SL**. Separation of liquid phases in giant vesicles of ternary mixtures of phospholipids and cholesterol. *Biophysical journal* 85: 3074–83, 2003.

121. **Widengren J, Schwille P**. Characterization of Photoinduced Isomerization and Back-Isomerization of the Cyanine Dye Cy5 by Fluorescence Correlation Spectroscopy. *The Journal of Physical Chemistry A* 104: 6416–6428, 2000.

122. **Wiggins P, Phillips R**. Analytic models for mechanotransduction: gating a mechanosensitive channel. *Proceedings of the National Academy of Sciences of the United States of America* 101: 4071–6, 2004.

123. **Van Zanten TS, Cambi A, Koopman M, Joosten B, Figdor CG, Garcia-Parajo MF**. Hotspots of GPI-anchored proteins and integrin nanoclusters function as nucleation sites for cell adhesion. *Proceedings of the National Academy of Sciences of the United States of America* 106: 18557–18562, 2009.

124. **Alberts**, Molecular Biology of the Cell. Garland Science. 2002.